

Microscopic theory of cavity-enhanced interactions of dipolaritons

E. R. Christensen,¹ A. Camacho-Guardian,² O. Cotlet,³ A. Imamoglu,³ M. Wouters,⁴ G. M. Bruun,^{1,5} and I. Carusotto⁶

¹*Center for Complex Quantum Systems, Department of Physics and Astronomy, Aarhus University, Ny Munkegade 120, DK-8000 Aarhus C, Denmark.*

²*Departamento de Física Química, Instituto de Física, Universidad Nacional Autónoma de México, Apartado Postal 20-364, Ciudad de México C.P. 01000, Mexico*

³*Institute for Quantum Electronics, ETH Zurich, Zurich, Switzerland*

⁴*TQC, Universiteit Antwerpen, Universiteitsplein 1, B-2610 Antwerp, Belgium*

⁵*Shenzhen Institute for Quantum Science and Engineering and Department of Physics, Southern University of Science and Technology, Shenzhen 518055, China.*

⁶*INO-CNR BEC and Dipartimento di Fisica Center, Università di Trento, Via Sommarive 14, I-38050 Povo, Trento, Italy*

(Dated: December 7, 2022)

We develop a theoretical model for the interaction strength between a pair of exciton-polaritons with finite and parallel static electric-dipole moments. In stark contrast to simple perturbative arguments predicting the interaction to be reduced due to the hybridisation with cavity photons, we find that the strong coupling to a cavity mode leads to a drastic enhancement of the polariton interactions as compared to bare excitons. This enhancement is caused by the small polariton mass due to its photonic component, which increases the kinetic cost associated with minimising the dipole-dipole repulsion. Microscopic numerical calculations for one-dimensional geometries show that the interaction strength for the lower polariton branch is maximal when the exciton and the cavity mode are close to resonance, and can easily exceed state-of-the-art cavity decay rates for realistic confinement lengths, thus entering the polariton blockade regime. Analytical extension of our results to two-dimensional polariton systems highlight dipolar polaritons as a most promising solid-state platform to realize strongly interacting photonic systems.

I. INTRODUCTION

The dramatic advances in experimental capabilities regarding hybrid light-matter quantum systems have opened the door to engineering systems that possess exotic phases of matter of fundamental interest and could serve as building blocks for future quantum technology [1, 2]. In this regard, microcavity exciton-polaritons (polaritons), namely bosonic quasiparticles that emerge from the strong coupling of an optical excitation of the material with a cavity photon mode in a semiconductor microcavity, have proven especially appealing. Characterized by an effective mass four orders of magnitude lower than the electron mass along with interactions inherited from their matter component, polaritons showcase a multitude of intrinsically interesting collective quantum phenomena such as non-equilibrium Bose-Einstein condensation [3, 4] and superfluidity [5, 6], and constitute promising candidates for realizing strongly correlated fluids of light [7–10]

A crucial step towards the realization of such quantum correlated states of matter is to achieve strong polariton-polariton interactions. This requires an enhancement of the interaction constant, which in turn calls for a microscopic understanding of the polariton-polariton scattering process. In the last decade, several pioneering theoretical and experimental studies have appeared on polariton interactions and enhanced polariton interactions compared to exciton ones have been predicted [11–24]. Yet, most of these studies have focused on excitons with a short range interaction, which significantly simplifies

the description of the scattering process.

A tempting strategy to reinforce polariton interaction is to use excitons possessing a static electric dipole. Such dipolar polaritons (dipolaritons) have been explored experimentally in different settings in quantum wells and optical wave guides [8, 25–28]. A thorough understanding of dipolar excitons calls for more sophisticated theoretical description due to the strength and range of the dipolar interaction.

Motivated by these exciting developments, in this article we develop a microscopic description of two polaritons interacting via their parallel dipole moments. As a measure of the strength of interactions, we numerically calculate the interaction-induced energy shift of the lowest two-particle state in a one-dimensional (1D) wire of finite length. In contrast to a naive expectation that the hybridisation of the excitons with the photons would decrease their interaction, a dramatic enhancement of the interaction strength is found: the reason is that the mass of the polaritons is much smaller than that of the excitons, which increases the kinetic energy cost associated with minimising the dipole-dipole repulsion.

In specific, three qualitatively different regimes emerge from our analysis: From a Tonks-Girardeau fermionization regime for long wires through an intermediate regime where the energy shift scales with the inverse wire length to a polariton blockade regime in short wires. The scaling laws exhibited by the results of our exact diagonalization are quantitatively recovered by a Born-Oppenheimer type approach, and allow to extend our theory to two di-

mensional systems. For traditional semiconductor-based devices, dipolaritons offer a moderate improvement of the interaction strength compared to standard contact-interacting polaritons. A sizable reinforcement is however predicted for tightly-bound excitons with a large oscillator strength, e.g. in 2D materials, and in multiple-well geometries. This enhancement is of great promise in view of realizing strongly correlated fluids of light in a solid-state platform.

The outline of the paper is as follows. In Sec. II, we present the model, and in Sec. III we give results for the ground state energy from exact diagonalization and discuss the different regimes determined by the wire length. We introduce the Born-Oppenheimer approach in Sec. IV, and Sec. V discusses the role of light coupling. In Sec. VI we use the Born-Oppenheimer approach to gain insight into different non-trivial scalings, and Sec. VII contains experimental considerations as well as comparisons between dipolaritons and non-dipolar polaritons. Finally, we provide concluding remarks in Sec. VIII. In the Appendices, we provide additional details regarding the Born-Oppenheimer model and on the peculiar dependence of the interaction energy on the exciton-photon detuning. We also provide additional numerical results for a slightly more sophisticated model of coupled direct- and indirect excitons, and for a mathematically similar quasi-1D coupled wire system.

II. MODEL

As illustrated in Fig. 1, we start by considering two dipolar excitons confined to a quantum wire and coupled to a cavity mode in an effectively 1D geometry. The dipole moment of the excitons is perpendicular to the wire giving rise to a strong repulsion, and we therefore expect that the short-range details of the excitons do not matter, which allows us to describe them as point-like particles [29].

The 1D dynamics along the quantum wire is described by the Hamiltonian

$$\begin{aligned} \hat{H} = & \sum_{k=1,2} \int dx_k \sum_{i,j \in \{C,X\}} \hat{\Psi}_i^\dagger(x_k) h_{ij}^0(x_k) \hat{\Psi}_j(x_k) \\ & + \frac{1}{2} \int dx_1 dx_2 [\hat{\Psi}_X^\dagger(x_1) \hat{\Psi}_X^\dagger(x_2) \\ & \times V_{dd}(|x_1 - x_2|) \hat{\Psi}_X(x_1) \hat{\Psi}_X(x_2)]. \end{aligned} \quad (1)$$

Here, h_{ij}^0 are the entries of the h^0 matrix

$$h^0(x_k) = \begin{pmatrix} -\frac{\hbar^2}{2m_C} \frac{\partial^2}{\partial x_k^2} + \Delta + \delta_C & \Omega \\ \Omega & -\frac{\hbar^2}{2m_X} \frac{\partial^2}{\partial x_k^2} \end{pmatrix}, \quad (2)$$

and we impose hard-wall boundary conditions at the edges $x_1, x_2 = 0, L$, of the wire. The exciton and cavity-photon masses are taken as $m_X = 2m_e$, i.e. twice the electron mass, and $m_C = 10^{-4} m_X$, respectively. The

corresponding field operators are $\hat{\Psi}_{X/C}$. The Rabi frequency Ω quantifies the strength of the exciton-photon coupling. In order to set the energy of the lowest photon mode on resonance with the exciton one, a detuning $\Delta = (m_X^{-1} - m_C^{-1}) \hbar^2 \pi^2 / (2L^2)$, is added to the photon energy. Any further detuning is contained in the parameter δ_C .

The dipolar interaction potential has the usual form

$$V_{dd}(x_1, x_2) = \frac{e^2 d^2}{4\pi\epsilon |x_1 - x_2|^3} \equiv \frac{C_3}{|x_1 - x_2|^3} \quad (3)$$

where e is the electron charge, ϵ is the dielectric constant of the material, and d is the spatial separation between electrons and holes in the exciton. In addition to coupled [25] and wide quantum wells [27] as well as TMD bilayers [30], such dipolar excitons have recently been realized in electrostatically-defined quasi-1D geometries [31]. If further embedded in a laterally confined, thus effectively one-dimensional microcavity, such a set-up could constitute a highly tunable platform to study 1D dipolaritons.

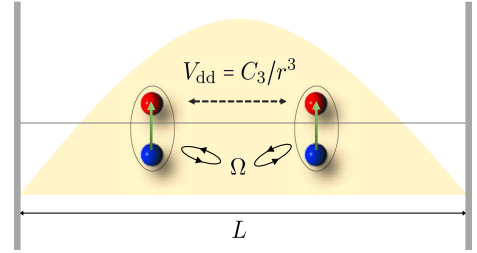


FIG. 1. Sketch of the system under consideration. Two dipolar excitons in a quantum wire (horizontal middle line) strongly coupled to a cavity photon mode (yellow wave). The dipole moment of the excitons is perpendicular to the wire leading to a strong repulsion.

Starting from the Hamiltonian (1), we numerically solve the two-body problem to obtain the exact ground state energy and wave function of two interacting dipolar polaritons. The ground state wave function is symmetric under particle exchange and has four components

$$\Psi(x_1, x_2) = \sum_{i,j \in \{C,X\}} \psi_{i,j}(x_1, x_2) \quad (4)$$

giving the excitonic and photonic amplitudes of the two polaritons. Since we are interested in varying the confinement length, L , across orders of magnitude and the dipolar potential varies strongly for small separation lengths, we diagonalise the Hamiltonian in Eq. (1) numerically by transforming to relative- and center of mass coordinates and discretising the spatial axes in a non-uniform grid [32]. Because of the large size of the Hamiltonian matrix, we only look for the lowest eigenvalue, E_{LP-LP} , with a Lanczos-type algorithm [33, 34]. We define the interaction energy as the difference between the interacting and non-interacting ground states of the two-particle

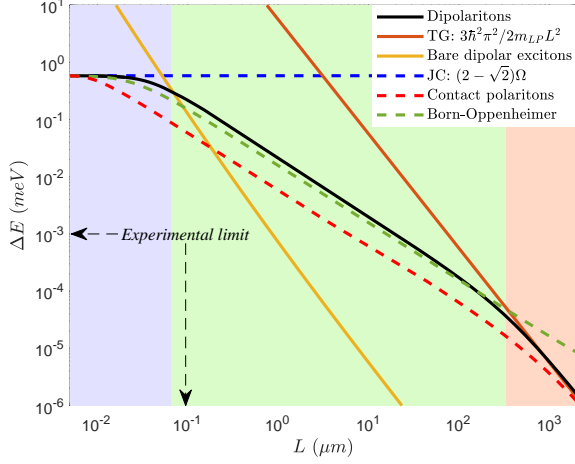


FIG. 2. Black solid line: Interaction energy of a pair of dipolaritons as a function of the confinement length L . For large L -values (right, red region), the interaction energy tends to the Tonks-Girardeau (TG) limit of two impenetrable bosons of mass $2m_C$ (red solid). For intermediate L -values (middle, green region), the energy shift is well-described by the perturbative Born-Oppenheimer (BO) model (green dashed). For small L -values (left, blue region) the energy shift approaches the Jaynes-Cummings (JC) regime of a zero-dimensional quantum dot (blue dashed horizontal). For intermediate to large confinement length (green and red regions), the interaction shift for the polaritons is larger than the one for bare dipolar excitons (lower orange full). A qualitatively similar behaviour is observed for contact-interacting polaritons (lower red dashed) with energy shift $\Delta E_{non-dip} \propto \Omega a_{exc}/L$, with a_{exc} the exciton Bohr radius set to 5 nm.

system, i.e.

$$\Delta E = E_{LP-LP} - 2E_{LP}. \quad (5)$$

If not otherwise specified, in all figures we set $d = 5$ nm, $\epsilon = 10\epsilon_0$, $\Omega = 1$ meV, and $\delta_C = 0$.

III. NUMERICAL RESULTS

In Fig. 2, the interaction energy ΔE is plotted as a function of the wire length L for the resonant case $\delta_C = 0$. Three regimes can be identified as a function of L .

A. Long wire regime

For a long wire, i.e. large L (right red region in Fig. 2), the interaction energy (black solid line) shows a $1/L^2$ scaling. This can be interpreted as the Tonks-Girardeau (TG) limit of two impenetrable hard-core bosonic polaritons [35, 36]: the dipolar interactions are strong enough to dominate over the kinetic energy and the polaritons get effectively fermionized. The physics is then fully determined by the impenetrability condition and does not

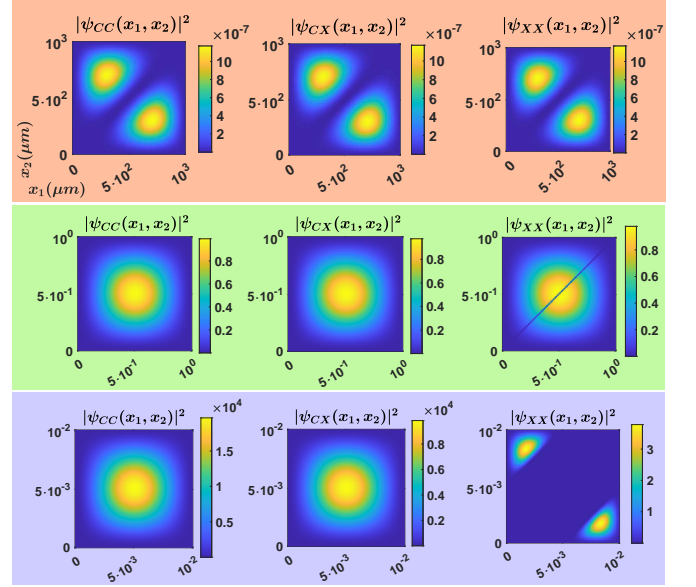


FIG. 3. Colorplots of the different components of the two-particle ground state wavefunction for different confinement lengths $L = 10^3 \mu\text{m}$ (top red panel), $L = 1 \mu\text{m}$ (middle green panel), and $L = 10^{-2} \mu\text{m}$ (bottom blue panel). Horizontal and vertical axes show x_1 and x_2 respectively, as shown for upper left panel. Left, center, right panels correspond to respectively the CC , $XC = CX$, XX components.

depend on the specific shape and range of the interaction potential. Quantitatively, the ground state energy $5\hbar^2\pi^2/[2(2m_C)L^2]$ is equal to that of two non-interacting *fermions* with *polariton mass* $m_{LP} = 2m_C$, which occupy the lowest ($n = 1$) and second lowest ($n = 2$) energy levels of the infinite square well of width L [37]. The interaction energy is obtained by subtracting twice the energy of the $n = 1$ state, which gives the result

$$\Delta E_{TG} = \frac{3\hbar^2\pi^2}{2(2m_C)L^2} \quad (6)$$

plotted as a red solid line in Fig. 2. To further corroborate this interpretation, the top row of Fig. 3 shows the absolute square of the normalized wavefunction components. This shows that in this large L regime, the entanglement of the photon and the exciton makes all four components have comparable weights and all vanish along the $x_1 \simeq x_2$ contact line, including the purely photonic one ψ_{CC} .

B. Short wire regime

In the opposite limit of a short wire shown by the blue region in Fig. 2, we observe a saturation of the interaction energy to a finite value. This can be understood as a Jaynes-Cummings (JC) regime [38, 39], where the electronic system behaves as a zero dimensional quantum dot and can only host a single matter excitation.

On the small L panels on the bottom row of Fig. 3, this is visible as a strong suppression of the two-exciton component ψ_{XX} by the blockade effect (right panel). Setting this component to zero, the Hamiltonian is readily diagonalized giving the ground state energy $-\sqrt{2}\Omega$ for the two-particle state. Since the energy of a single lower polariton is $-\Omega$, it follows that the interaction energy is

$$\Delta E_{JC} = (2 - \sqrt{2})\Omega. \quad (7)$$

Equation (7) is plotted as a horizontal blue dashed line in Fig. 2.

C. Intermediate wire length regime

The physics is richest for intermediate wire lengths L shown by the central green panel in Fig. 2. As one can hint on the figure, here the interaction energy displays a $1/L$ scaling typical of weakly interacting bosons [37], to be contrasted to the $1/L^2$ scaling of the impenetrable boson case discussed above for the large L regime.

The $1/L$ scaling can be qualitatively understood in terms of the effective potential that the polaritons inherit from the dipole-dipole interaction between their excitonic components. Following the JC argument above, we can approximate this potential as a barrier of height $(2 - \sqrt{2})\Omega$ and range set by the distance where the dipolar interaction energy equals the Rabi coupling, namely $R = (C_3/\Omega)^{1/3}$. At a perturbative Born-approximation level, this simple argument results in an estimate for the interaction energy

$$\Delta E_{interm} \propto \frac{\Omega^{2/3} C_3^{1/3}}{L} \quad (8)$$

which recovers the functional trend found in the numerics. A more rigorous and quantitative derivation of this key result, and a detailed analysis of its parameter dependence will be presented in the next section.

Using Eqs. (6)-(8), we can estimate the cross-over between the regime of long and intermediate wire lengths to occur at $L \sim (m\Omega^{2/3}C_3^{1/3})^{-1}$, whereas the cross-over between the short and intermediate regimes is at $L \sim C_3^{1/3}/\Omega^{1/3}$.

IV. BORN-OPPENHEIMER ENERGY LANDSCAPES

In order to put our interpretation of the intermediate regime on a solid quantitative basis, we perform a Born-Oppenheimer (BO) like approximation inspired by molecular physics and consider an effective potential landscape determined by the energy of the ground state of two particles located at a fixed distance $r = |x_1 - x_2|$. This can be calculated by diagonalizing the 4×4 matrix that describes the two-particle problem in

the CC, XC, CX, XX basis, where interactions are included as an energy shift of the XX state by the dipolar potential $V_{dd}(r)$ while the kinetic energy is neglected, see App. A for details. This approach is expected to be valid as long as the kinetic energy is smaller than the splitting of the BO energy landscapes.

The energies of the three symmetric eigenstates under particle-exchange are plotted in Fig. 4 as a function of r . For large r values the eigenenergies recover the ones of the three combinations of non-interacting lower (LP) and upper (UP) polaritons. For smaller r , the dipolar potential (green dashed) becomes important and the eigenenergies are shifted up in energy. On the one hand, the highest energy state (red solid) tends to a pair of repulsively interacting excitons and thus diverges as the dipolar potential. On the other hand, the shift of the lowest energy state (black solid) saturates to a finite value $(2 - \sqrt{2})\Omega$ determined by the JC energy shift: for such small distances, the dipolar potential is large enough to suppress the coupling to the XX state. As expected, the size of this saturation region compares qualitatively well with the value of the dipolar radius R introduced in the previous Section.

A prediction for the interaction energy of a pair of dipolaritons can now be extracted by evaluating the expectation value of the BO energy in the non-interacting ground state wavefunction. Such a perturbative estimate is expected to be accurate when the wire is short so that the energy gap to the next confined state well exceeds the interaction energy. The result, plotted as dashed green line in Fig. 2, captures in a quantitatively accurate way the full numerical calculation (black solid) except in the large L region. It is important to note that this result stems from the application of perturbation theory to the non-perturbative BO energy landscapes. In contrast to most previous works on polariton-polariton interactions [11–13, 17], the result is therefore fully non-perturbative in the exciton interaction potential. The slight deviation at relatively small L values around the blue/green interface stems from corrections to the BO model due to kinetic energy effects.

For even smaller L (blue region), the simple BO model perfectly recovers the JC energy shift in the quantum dot limit. This interpretation is further confirmed in the middle row of Fig. 3 for an intermediate $L = 1 \mu\text{m}$: as expected from the BO energy landscape, the ground state closely resembles the product of free-particle sine-shaped wavefunctions with a narrow depression along the contact line in the XX -component only. Physically, this reflects the fact that when the polaritons are too close, one of them is forced to break into a pure cavity photon.

V. ROLE OF STRONG COUPLING WITH LIGHT

At the perturbative level, one would expect the light coupling to reduce the interaction between the polaritons

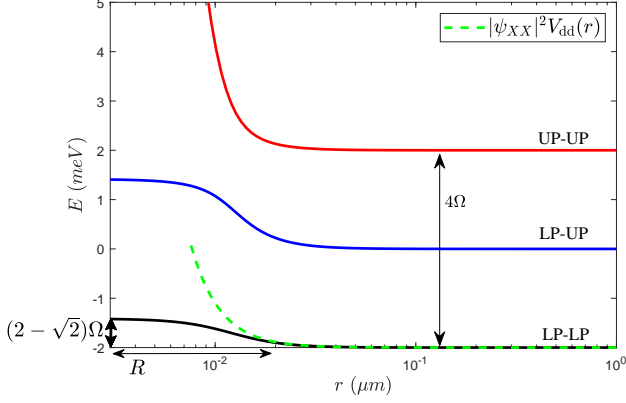


FIG. 4. Born-Oppenheimer energy landscapes as a function of the separation r between the polaritons. The green dashed line indicates the dipolar potential between bare excitons weighted by the Hopfield coefficient.

by the factor $|u_X|^4$ where u_X is the excitonic Hopfield coefficient, as compared to that between bare dipolar excitons. Our numerics find a completely different behaviour, with much stronger interactions between polaritons than between bare excitons. The reason of this exciting behaviour is that hybridisation with light makes polariton mass much smaller than the exciton one. This in turn increases the kinetic energy cost of localisation to minimise the interaction energy. This key result is easily appreciated by comparing in Fig. 2 the interaction energy of a pair of dipolaritons with that of two bare excitons interacting via the same dipolar potential (yellow lower solid).

The enhancement of the interaction strength is most visible in the large L limit governed by TG physics (red region), where the lighter mass of dipolaritons provides a $m_X/m_C \sim 10^4$ enhancement factor of the kinetic energy. A marked enhancement is also visible in the intermediate regime (green middle region), again due to the kinetic energy of the photonic component. Only for unrealistically short wires, the coupling to light leads to a reduction of the effective strength of interaction by allowing excitons to avoid overlapping by turning one of the polaritons into a photon.

VI. DEPENDENCE ON PARAMETERS

Further insight into the physics of our model can be obtained by means of a closer look at the scaling of the interaction energy with the system parameters.

In Fig. 5 we plot the interaction energy as a function of Ω (top left) and of the dipolar strength C_3 (top right) for $L = 1 \mu\text{m}$ corresponding to the most relevant intermediate wire length regime. The two panels confirm the $\Omega^{2/3}$ and $C_3^{1/3}$ behaviors predicted by the simple argument underlying Eq. (8) and highlight the crucial role of the Rabi coupling Ω in the interaction process.

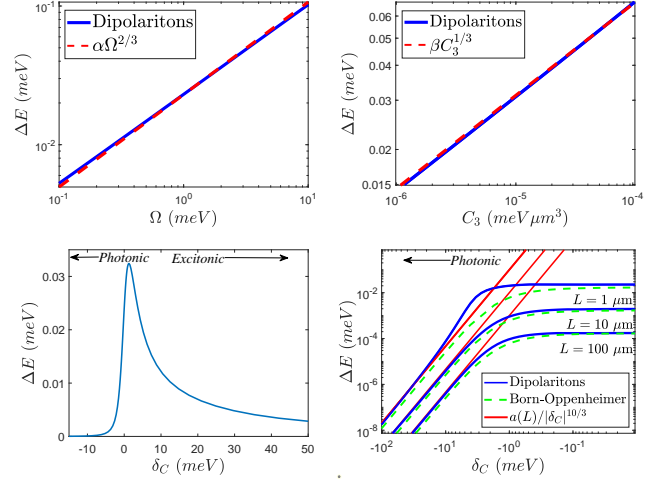


FIG. 5. Numerical calculation (solid blue) and power-law analytical fit (red dashed) for the energy shift at fixed $L = 1 \mu\text{m}$ as function of Rabi coupling Ω (top left), of dipolar strength C_3 (top right) and as function of detuning δ_C in linear (bottom left) and log-log (bottom right) scales. Here, larger L -values are also shown and the solid red and green dashed lines indicate the BO approximation and the analytical fit respectively.

To assess how the exciton-photon detuning δ_C influences the interaction energy, we plot in the bottom left panel of Fig. 5 ΔE as a function of detuning for $L = 1 \mu\text{m}$ and $\Omega = 1 \text{ meV}$. The most apparent feature is that the interaction energy reaches its maximum in the vicinity of the $\delta_C = 0$ resonance condition. This result is to be contrasted with the naive argument of standard perturbation theory that interactions scale with the excitonic Hopfield coefficient as $\Delta E \sim |u_X|^4$ and are maximum on the far excitonic side at large and positive δ_C . Once again, this confirms the key role played by the kinetic energy of the photonic component in reinforcing the interaction energy.

For $\delta_C > 0$, the interaction energy decays towards the much smaller value for two bare excitons in the TG regime, $3\hbar^2\pi^2/(2m_X L^2)$. As discussed in App. B1, the first correction to this asymptotic value comes from the mixing of excitons with the much lighter photons, which gives a contribution to the effective mass $\propto 1/\delta_C^2$.

For large negative detunings $\delta_C < 0$, the system is mostly photonic and the energy shift again drops to zero. To pin down the δ_C -dependence on the negative side, we display in the bottom right panel of Fig. 5 a log-log plot of the interaction energy as function of (negative) δ_C for different values of L . For large and negative δ_C , the dependence displays a very non-trivial $|\delta_C|^{-10/3}$ law (green dashed lines) which differs from all previous models. A justification of this unexpected scaling is given in App. B2 in terms of the BO model.

We emphasize how this $|\delta_C|^{-10/3}$ dependence is different from the one that one would expect from a naive Born-approximation calculation for which the interaction potential for polaritons is proportional to the $|u_X|^4$ Hopfield coefficient and, therefore, to $(\Omega/\delta_C)^4$ [5]. Within our

theory, this dependence is also peculiar to the dipolariton case: for polaritons emerging from contact-interacting excitons, the radius of the potential peak is in fact fixed by the exciton radius, so the interaction energy scales in a slightly slower way as $|\delta_C|^{-3}$. Interestingly, this result recovers the prediction of the standard model for the nonlinearity stemming from saturation of the excitonic oscillator strength, proportional to the $u_X^3 u_C$ Hopfield coefficients [5].

VII. EXPERIMENTAL CONSIDERATIONS

We conclude our work with a discussion of actual experimental observability of our predictions and of their relevance for the on-going quest for realising strongly correlated polariton fluids.

From Fig. 2, it appears that the TG regime is hardly observable in state-of-the-art wire devices whose linewidth γ is typically on the μeV range at the very best [40]. On the contrary, effective polariton blockade $\Delta E > \gamma$ is expected to be within reach in confined wire geometries of μm -range length with realistically narrow linewidths, where the findings of Fig. 2 suggest that dipolaritons offer a significant advantage compared to standard contact-interacting polaritons (dashed red curve).

A. Two-dimensional systems

To go beyond 1D systems and get insight on experimentally most relevant 2D geometries, we take advantage of the analytical understanding extracted from the 1D calculations and extend the BO theory to higher dimensions. Figure 2 shows how our full numerics are well recovered by the perturbation theory based on the BO potential, while the calculations in App. D show how the BO model is quantitatively accurate also for a coupled-wire geometry. All this supports that the BO model is valid independently of the geometry and the dimensionality.

For a generic D -dimensional model, the BO model gives a dipolariton interaction energy that scales as

$$\Delta E_D \propto \Omega R^D / L^D = \Omega^{1-D/3} C_3^{D/3} / L^D. \quad (9)$$

As a most salient feature, this scaling implies that for any $D \leq 2$ the interaction energy grows with Ω , which implies that, for fixed dipolar length d and dipolar interaction strength C_3 , more tightly-bound excitons with a stronger oscillator strength are favourable in view of achieving strong interactions. As opposed to the one-dimensional case, we note that for $D = 2$ there is no clear division between interaction- and kinetic energy dominated regimes as function of confinement length since both shifts scale as $1/L^2$. However, this crossover can be accessed by tuning the parameters Ω , C_3 and δ_C .

The dipolariton interaction-induced scaling is to be contrasted with non-dipolar polaritons where interactions are stronger for Wannier excitons with a large Bohr radius a_{exc} . In this case, a_{exc} (and not the length R) sets the radius of the effective hard-core potential shown in Fig. 4. It follows that the two-polariton interaction energy scales as $\Delta E_{\text{non-dip}} \propto \Omega a_{\text{exc}}^D / L^D$. Since the Rabi coupling scales as $\Omega \sim a_{\text{exc}}^{-D/2}$, the resulting interaction energy scales as $\Delta E_{\text{non-dip}} \propto a_{\text{exc}}^{D/2} \propto 1/\Omega$ which manifestly favors Wannier excitons with a large Bohr radius.

B. Quantitative remarks

For typical parameter values of GaAs-based devices used in this paper with $\Omega = 1 \text{ meV}$, a dipolar length $d = 5 \text{ nm}$ and an exciton radius $a_{\text{exc}} = 5 \text{ nm}$, we have $R \simeq 15 \text{ nm}$ and the interaction energy of dipolar polaritons is a factor of ~ 3 (in 1D) and ~ 9 (in 2D) larger than the non-dipolar one and is on the edge of photon blockade already for realistic pillars of $1 \mu\text{m}$ area.

Furthermore, in contrast to non-dipolar polaritons, the scaling in Eq. 9 predicts a wide margin for further improvement in the dipolar case by using, e.g., dipolar excitons in two-dimensional transition metal dichalcogenide (TMD) materials or Frenkel excitons in organic materials where excitons are much more tightly bound. [41, 42]. Of course, this conclusion holds provided a similar value of the dipolar length d can be obtained also for stronger bound excitons. This could be realised, e.g., in a two-layer set-up with a layer separation larger the exciton Bohr radius and, at the same time, a strong tunnel coupling of electrons or holes between two layers. In this case, the hybridized intra-layer and inter-layer excitons could ensure concurrently a large Ω (due to intra-layer component of the hybrid exciton) while maintaining a large dipole moment (due to inter-layer component) [25, 43]. Evidence of excitons with a sizable oscillator strength and, at the same time, a large spatial size has been reported in [31].

Thanks to the spatially long-range shape of the dipolar interactions, a further increase of Ω can be obtained using N quantum wells, or TMD monolayers separated by few layers of hBN. In standard non-dipolar polaritons, an increase in Ω would be in fact compensated by the reduced interactions between delocalized excitons in the N wells/layers. For dipolaritons with typical dipolar interaction range R in the 10 nm range, several electronically disconnected layers could be placed such that the vertical distance between the first and last layer is smaller than R . Here, inter-layer and intra-layer dipolar exciton interactions would be comparable, and dipolar interactions would be able to block excitons in every pair of layers. This results in a factor of \sqrt{N} increase of Ω which from Eq. 9 gives an overall $N^{(1-D/3)/2}$ increase of the interaction energy. All together, these improvements should be sufficient to bring dipolariton systems [8] into the regime of strong interactions.

VIII. CONCLUSIONS AND OUTLOOK

In this article we have developed a microscopic model of the interactions between dipolar polaritons in a 1D geometry. Depending on the wire length, different regimes are identified, from a single-mode quantum dot-like behaviour in short wires, to impenetrable polaritons in long ones. The physically most relevant regime lies in between and can be quantitatively described in terms of perturbation theory using an effective Born-Oppenheimer potential. In particular, our work highlights the crucial role of the light-matter coupling in increasing interactions between polaritons over bare exciton ones for physically relevant wire lengths. Further theoretical work will address the extension of our theory to Rydberg polaritons propagating in atomic gases and semiconductor microcavities which have been recently demonstrated [44–48] as a promising alternative platform for strongly interacting polaritons, albeit in a conceptually different propagating geometry for atomic gases [49].

In addition to its theoretical interest as the first microscopic model polariton interactions, our results have the

strong experimental interest of suggesting dipolaritons emerging from tightly bound excitons in TMDs and/or in multiple quantum well geometries as a promising candidate for achieving strong interactions. Such a result would open a new era in the study of strongly correlated fluids of light using state-of-the-art semiconductor optics technology.

ACKNOWLEDGMENTS

We acknowledge financial support from the Danish National Research Foundation through the Center of Excellence “CCQ” (Grant agreement no.: DNRFF156) and the U.S. Army CCDC Atlantic Basic and Applied Research via Grant No. W911NF-19-1-0403. The work at ETH Zurich was supported by the Swiss National Science Foundation (SNSF) under Grant Number 200020_207520. I. Carusotto acknowledges financial support from the European Union H2020-FETFLAG-2018-2020 project “PhoQuS” (n.820392), from the Provincia Autonoma di Trento, and from the Q@TN initiative. We also thank Deepnakur Thureja, Puneet Murty, Daniele De Bernardis and Thomas Pohl for many discussions.

-
- [1] Darrick E. Chang, Vladan Vuletić, and Mikhail D. Lukin, “Quantum nonlinear optics – photon by photon,” *Nature Photonics* **8**, 685–694 (2014).
 - [2] Gershon Kurizki, Patrice Bertet, Yuimaru Kubo, Klaus Mølmer, David Petrosyan, Peter Rabl, and Jörg Schmiedmayer, “Quantum technologies with hybrid systems,” *Proceedings of the National Academy of Sciences* **112**, 3866–3873 (2015).
 - [3] Jacqueline Bloch, Iacopo Carusotto, and Michiel Wouters, “Non-equilibrium bose–einstein condensation in photonic systems,” *Nature Reviews Physics* **4**, 470–488 (2022).
 - [4] Quentin Fontaine, Davide Squizzato, Florent Baboux, Ivan Amelio, Aristide Lemaître, Martina Morassi, Isabelle Sagnes, Luc Le Gratiet, Abdelmounaim Harouri, Michiel Wouters, Iacopo Carusotto, Alberto Amo, Maxime Richard, Anna Minguzzi, Léonie Canet, Sylvain Ravets, and Jacqueline Bloch, “Kardar–parisi–zhang universality in a one-dimensional polariton condensate,” *Nature* **608**, 687–691 (2022).
 - [5] Iacopo Carusotto and Cristiano Ciuti, “Quantum fluids of light,” *Rev. Mod. Phys.* **85**, 299–366 (2013).
 - [6] Alberto Amo, Jérôme Lefrère, Simon Pigeon, Claire Adrados, Cristiano Ciuti, Iacopo Carusotto, Romuald Houdré, Elisabeth Jacobino, and Alberto Bramati, “Superfluidity of polaritons in semiconductor microcavities,” *Nature Physics* **5**, 805 EP – (2009).
 - [7] A. Verger, C. Ciuti, and I. Carusotto, “Polariton quantum blockade in a photonic dot,” *Phys. Rev. B* **73**, 193306 (2006).
 - [8] Emre Togan, Hyang-Tag Lim, Stefan Faelt, Werner Wegscheider, and Atac Imamoglu, “Enhanced interactions between dipolar polaritons,” *Phys. Rev. Lett.* **121**, 227402 (2018).
 - [9] Aymeric Delteil, Thomas Fink, Anne Schade, Sven Höfling, Christian Schneider, and Ataç İmamoglu, “Towards polariton blockade of confined exciton–polaritons,” *Nature Materials* **18**, 219–222 (2019).
 - [10] Guillermo Muñoz-Matutano, Andrew Wood, Mattias Johnsson, Xavier Vidal, Ben Q. Baragiola, Andreas Reinhard, Aristide Lemaître, Jacqueline Bloch, Alberto Amo, Gilles Nogues, Benjamin Besga, Maxime Richard, and Thomas Volz, “Emergence of quantum correlations from interacting fibre-cavity polaritons,” *Nature Materials* **18**, 213–218 (2019).
 - [11] C. Ciuti, V. Savona, C. Piermarocchi, A. Quattropani, and P. Schwendimann, “Role of the exchange of carriers in elastic exciton–exciton scattering in quantum wells,” *Phys. Rev. B* **58**, 7926–7933 (1998).
 - [12] G. Rochat, C. Ciuti, V. Savona, C. Piermarocchi, A. Quattropani, and P. Schwendimann, “Excitonic bloch equations for a two-dimensional system of interacting excitons,” *Phys. Rev. B* **61**, 13856–13862 (2000).
 - [13] M. M. Glazov, H. Ouerdane, L. Pilozi, G. Malpuech, A. V. Kavokin, and A. D’Andrea, “Polariton-polariton scattering in microcavities: A microscopic theory,” *Phys. Rev. B* **80**, 155306 (2009).
 - [14] Michiel Wouters, “Resonant polariton-polariton scattering in semiconductor microcavities,” *Phys. Rev. B* **76**, 045319 (2007).
 - [15] I. Carusotto, T. Volz, and A. Imamoglu, “Feshbach blockade: Single-photon nonlinear optics using resonantly enhanced cavity polariton scattering from biexciton states,” *EPL (Europhysics Letters)* **90**, 37001 (2010).
 - [16] N. Takemura, S. Trebaol, M. Wouters, M. T. Portella-Oberli, and B. Deveaud, “Polaritonic feshbach reso-

- nance,” *Nature Physics* **10**, 500–504 (2014).
- [17] E. Estrecho, T. Gao, N. Bobrovska, D. Comber-Todd, M. D. Fraser, M. Steger, K. West, L. N. Pfeiffer, J. Levinsen, M. M. Parish, T. C. H. Liew, M. Matuszewski, D. W. Snoke, A. G. Truscott, and E. A. Ostrovskaya, “Direct measurement of polariton-polariton interaction strength in the thomas-fermi regime of exciton-polariton condensation,” *Phys. Rev. B* **100**, 035306 (2019).
 - [18] Jesper Levinsen, Francesca Maria Marchetti, Jonathan Keeling, and Meera M. Parish, “Spectroscopic signatures of quantum many-body correlations in polariton microcavities,” *Phys. Rev. Lett.* **123**, 266401 (2019).
 - [19] Hui Hu, Hui Deng, and Xia-Ji Liu, “Polariton-polariton interaction beyond the born approximation: A toy model study,” *Phys. Rev. A* **102**, 063305 (2020).
 - [20] A. Camacho-Guardian, M. A. Bastarrachea-Magnani, and G. M. Bruun, “Mediated interactions and photon bound states in an exciton-polariton mixture,” *Phys. Rev. Lett.* **126**, 017401 (2021).
 - [21] Miguel A. Bastarrachea-Magnani, Arturo Camacho-Guardian, and Georg M. Bruun, “Attractive and repulsive exciton-polariton interactions mediated by an electron gas,” *Phys. Rev. Lett.* **126**, 127405 (2021).
 - [22] A. Camacho-Guardian, M. Bastarrachea-Magnani, T. Pohl, and G. M. Bruun, “Strong photon interactions from weakly interacting particles,” *Phys. Rev. B* **106**, L081302 (2022).
 - [23] Olivier Bleu, Guangyao Li, Jesper Levinsen, and Meera M. Parish, “Polariton interactions in microcavities with atomically thin semiconductor layers,” *Phys. Rev. Research* **2**, 043185 (2020).
 - [24] Guangyao Li, Meera M. Parish, and Jesper Levinsen, “Microscopic calculation of polariton scattering in semiconductor microcavities,” *Phys. Rev. B* **104**, 245404 (2021).
 - [25] Peter Cristofolini, Gabriel Christmann, Simeon I. Tsintzos, George Deligeorgis, George Konstantinidis, Zacharias Hatzopoulos, Pavlos G. Savvidis, and Jeremy J. Baumberg, “Coupling quantum tunneling with cavity photons,” *Science* **336**, 704–707 (2012).
 - [26] Tim Byrnes, German V. Kolmakov, Roman Ya. Kezerašvili, and Yoshihisa Yamamoto, “Effective interaction and condensation of dipolaritons in coupled quantum wells,” *Phys. Rev. B* **90**, 125314 (2014).
 - [27] Itamar Rosenberg, Yotam Mazuz-Harpaz, Ronen Rapaport, Kenneth West, and Loren Pfeiffer, “Electrically controlled mutual interactions of flying waveguide dipolaritons,” *Phys. Rev. B* **93**, 195151 (2016).
 - [28] Itamar Rosenberg, Dror Liran, Yotam Mazuz-Harpaz, Kenneth West, Loren Pfeiffer, and Ronen Rapaport, “Strongly interacting dipolar-polaritons,” *Science Advances* **4**, eaat8880 (2018).
 - [29] Hongyi Yu and Wang Yao, “Luminescence anomaly of dipolar valley excitons in homobilayer semiconductor moiré superlattices,” *Phys. Rev. X* **11**, 021042 (2021).
 - [30] Biswajit Datta, Mandeep Khatoniar, Prathmesh Deshmukh, Félix Thouin, Rezlind Bushati, Simone De Liberato, Stephane Kena Cohen, and Vinod M Menon, “Highly nonlinear dipolar exciton-polaritons in bilayer mos_2 ,” *Nature communications* **13**, 1–7 (2022).
 - [31] Deepankur Thureja, Atac Imamoglu, Tomasz Smolenski, Alexander Popert, Thibault Chervy, Xiaobo Lu, Song Liu, Katayun Barmak, Kenji Watanabe, Takashi Taniguchi, David J. Norris, Martin Kroner, and Puneet A. Murthy, “Tunable quantum confinement of neutral excitons using electric fields and exciton-charge interactions,” (2022), [arXiv:2102.08989 \[cond-mat.mes-hall\]](https://arxiv.org/abs/2102.08989).
 - [32] I.-H. Tan, Gregory L. Snider, L. D. Chang, and Evelyn L. Hu, “A self-consistent solution of schrödinger–poisson equations using a nonuniform mesh,” *Journal of Applied Physics* **68**, 4071–4076 (1990).
 - [33] Cornelius Lanczos, “An iteration method for the solution of the eigenvalue problem of linear differential and integral operators,” *Journal of research of the National Bureau of Standards* **45**, 255–282 (1950).
 - [34] G. W. Stewart, “A krylov–schur algorithm for large eigenproblems,” *SIAM Journal on Matrix Analysis and Applications* **23**, 601–614 (2002).
 - [35] Lewi Tonks, “The complete equation of state of one, two and three-dimensional gases of hard elastic spheres,” *Phys. Rev.* **50**, 955–963 (1936).
 - [36] M. Girardeau, “Relationship between systems of impenetrable bosons and fermions in one dimension,” *Journal of Mathematical Physics* **1**, 516–523 (1960), <https://doi.org/10.1063/1.1703687>.
 - [37] Elliott H. Lieb and Werner Liniger, “Exact analysis of an interacting bose gas. i. the general solution and the ground state,” *Phys. Rev.* **130**, 1605–1616 (1963).
 - [38] E.T. Jaynes and F.W. Cummings, “Comparison of quantum and semiclassical radiation theories with application to the beam maser,” *Proceedings of the IEEE* **51**, 89–109 (1963).
 - [39] L. Tian and H. J. Carmichael, “Quantum trajectory simulations of two-state behavior in an optical cavity containing one atom,” *Phys. Rev. A* **46**, R6801–R6804 (1992).
 - [40] Yongbao Sun, Patrick Wen, Yoseob Yoon, Gangqiang Liu, Mark Steger, Loren N. Pfeiffer, Ken West, David W. Snoke, and Keith A. Nelson, “Bose-einstein condensation of long-lifetime polaritons in thermal equilibrium,” *Phys. Rev. Lett.* **118**, 016602 (2017).
 - [41] Thomas Mueller and Ermin Malic, “Exciton physics and device application of two-dimensional transition metal dichalcogenide semiconductors,” *npj 2D Materials and Applications* **2**, 29 (2018).
 - [42] M. Knupfer, “Exciton binding energies in organic semiconductors,” *Applied Physics A* **77**, 623–626 (2003).
 - [43] VM Agranovich, DM Basko, GC La Rocca, and Franco Bassani, “Excitons and optical nonlinearities in hybrid organic-inorganic nanostructures,” *Journal of Physics: Condensed Matter* **10**, 9369 (1998).
 - [44] Thibault Peyronel, Ofer Firstenberg, Qi-Yu Liang, Sebastian Hofferberth, Alexey V Gorshkov, Thomas Pohl, Mikhail D Lukin, and Vladan Vuletić, “Quantum nonlinear optics with single photons enabled by strongly interacting atoms,” *Nature* **488**, 57–60 (2012).
 - [45] Alexey V. Gorshkov, Johannes Otterbach, Michael Fleischhauer, Thomas Pohl, and Mikhail D. Lukin, “Photon-photon interactions via rydberg blockade,” *Phys. Rev. Lett.* **107**, 133602 (2011).
 - [46] Ofer Firstenberg, Thibault Peyronel, Qi-Yu Liang, Alexey V Gorshkov, Mikhail D Lukin, and Vladan Vuletić, “Attractive photons in a quantum nonlinear medium,” *Nature* **502**, 71–75 (2013).
 - [47] Valentin Walther, Robert John, and Thomas Pohl, “Giant optical nonlinearities from rydberg excitons in semiconductor microcavities,” *Nature Communications*

- [9, 1309 \(2018\)](#).
 [48] Konstantinos Orfanakis, Sai Kiran Rajendran, Valentin Walther, Thomas Volz, Thomas Pohl, and Hamid Ohadi, “Rydberg exciton–polaritons in a cu2o microcavity,” *Nature Materials* **21**, 767–772 (2022).
 [49] Pierre-Élie Larré and Iacopo Carusotto, “Propagation of a quantum fluid of light in a cavityless nonlinear optical medium: General theory and response to quantum quenches,” *Physical Review A* **92**, 043802 (2015).

Appendix A: Details on the Born-Oppenheimer approximation

Here we give additional technical details on the Born-Oppenheimer approximation discussed in the main text. To this purpose, we consider the 4-by-4 matrix:

$$h_{BO} = \begin{pmatrix} 2(\epsilon_{C,1} + \Delta + \delta_C) & \Omega & \Omega & 0 \\ \Omega & \epsilon_{C,1} + \Delta + \delta_C + \epsilon_{X,1} & 0 & \Omega \\ \Omega & 0 & \epsilon_{C,1} + \Delta + \delta_C + \epsilon_{X,1} & \Omega \\ 0 & \Omega & \Omega & 2\epsilon_{X,1} + V_{dd}(r) \end{pmatrix} \quad (A1)$$

where r is the separation between the two particles, and $\Delta = \epsilon_{X,1} - \epsilon_{C,1}$, meaning that $\delta_C = 0$ is the resonance.

The Born-Oppenheimer energy landscapes $V_{BO,i}$ shown in Fig. 4 of the main text are obtained by calculating the eigenvalues of h_{BO} as a function of the distance r . As we are dealing with bosonic particles, we can restrict to the symmetric subspace under exchange of the two particles, which reduces the basis to the states CC , XX and $XC + CX$ states. In particular, the lowest eigenvalue describes the effective interaction potential V_{BO} between a pair of lower polaritons. To calculate the energy shift of the ground state in the confinement potential, perturbation theory prescribes that we calculate

$$\Delta E = \int_0^L \int_0^L dx_1 dx_2 V_{BO}(x_1 - x_2) |\psi_{LP}(x_1)|^2 |\psi_{LP}(x_2)|^2, \quad (A2)$$

where $|\psi_{LP}(x_1)|^2$ is the absolute square of the non-interacting lower-polariton wavefunction in the box.

Most remarkably, even though this calculation is perturbative in the effective Born-Oppenheimer interaction potential V_{BO} , it is not perturbative in the underlying exciton-exciton interaction potential.

Appendix B: Dependence of the interaction energy on the exciton-photon detuning

1. Positive detuning

In Fig. 6, we show the numerically calculated dependence on positive detuning of the system of cavity photon and dipolar exciton in a strictly 1D geometry as discussed in the main text. For this configuration, we have seen in Fig. 5 of the main manuscript that for large positive detunings δ_C , the energy tends to the energy of two interacting bare excitons. This behaviour is shown in greater detail in Fig. 6 for different values of L .

It is seen that for a large L in the TG-regime, the interaction energy indeed decreases following the dependence of the effective lower polariton mass, $m_{LP}^{-1} \simeq m_X^{-1} + m_C^{-1} \frac{\Omega^2}{\delta_C^2}$, with a $1/\delta_C^2$ slope followed by an asymptotically constant value. For the smallest $L = 1 \mu\text{m}$, the picture is more complicated but in all cases the energy shift saturates to an energy given by the sum of the TG energy for bare excitons and the corresponding average value of the dipole-dipole potential. All these scaling considerations directly extend to the case of polaritons emerging from contact-interacting excitons.

2. Negative detuning

As mentioned in the main text, the dependence for negative detuning as $|\delta_c|^{10/3}$ shown in the bottom right panel of Fig. 5 is even more intriguing. To understand it within the BO picture, we first need to estimate the height of the potential peak around $r = 0$ on the green curve in Fig. 4. To this purpose, we need to compare the asymptotic energy of two LPs at infinity with the $r = 0$ value. These are obtained as the lowest eigenvalue of the 3-by-3 matrix describing the projection of the BO Hamiltonian on the symmetric subspace,

$$\begin{pmatrix} 2\delta_C & \sqrt{2}\Omega & 0 \\ \sqrt{2}\Omega & \delta_C & \sqrt{2}\Omega \\ 0 & \sqrt{2}\Omega & V_{\text{dip}}(r) \end{pmatrix} \quad (B1)$$

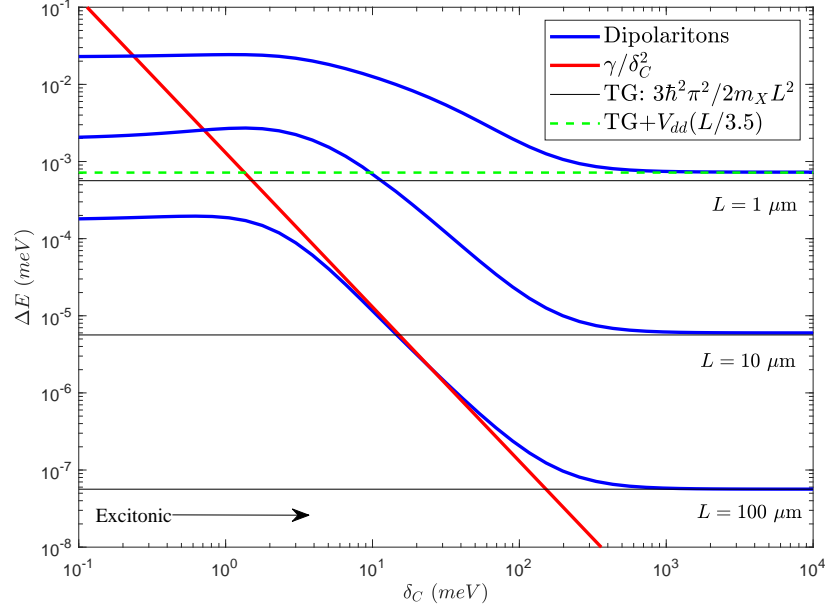


FIG. 6. Energy shift as function of positive detuning δ_C for different confinement lengths.

At $r = 0$, the dipolar potential is infinite, so we can restrict to the first and second rows and columns, obtaining, in the large and negative δ_C limit

$$E_{r=0} = 2\delta_C + \frac{2\Omega^2}{\delta_C} - \frac{4\Omega^4}{\delta_C^3} \quad (\text{B2})$$

At $r = \infty$, particles are non-interacting, so the asymptotic energy is equal to twice the single LP energy, $E_{r=\infty} = 2E_{LP}$ with

$$E_{LP} = \delta_C + \frac{\Omega^2}{\delta_C} - \frac{\Omega^4}{\delta_C^3} \quad (\text{B3})$$

Taking the difference of the two quantities gives a dependence as

$$E(r=0) - E(r=\infty) \simeq \frac{2\Omega^4}{|\delta_C^3|}. \quad (\text{B4})$$

An estimate of the expectation value of the interaction energy on the ground state is obtained by multiplying the peak potential times the effective radius R_{δ_C} . Since the energy scale on the diagonal of the matrix (B1) is δ_C , the characteristic radius can be estimated as $R_{\delta_C} \sim (C_3/\delta_C)^{1/3}$. Multiplied to the dependence in (B4), this provides a physical explanation to the overall $|\delta_C|^{-10/3}$ observed in the bottom right panel of Fig. 5.

Appendix C: Model with direct and indirect excitons

The validity of simplest model considered in the main text is confirmed by a calculation for a physically realistic model that is inspired from recent literature on coupled quantum wells [25] and explicitly involves two different types of excitons, direct- and indirect. In this model, the two excitonic species are coupled by a tunnel-like coupling term and only the indirect exciton has a permanent dipole moment which gives rise to the dipole-dipole repulsion in the two-particle problem.

The Hamiltonian has the form

$$\hat{H} = \sum_{k=1,2} \int dx_k \sum_{i,j=\{C,X,IX\}} \hat{\Psi}_i^\dagger(x_k) h_{ij}^0(x_k) \hat{\Psi}_j(x_k) + \frac{1}{2} \int dx_1 dx_2 [\hat{\Psi}_{IX}^\dagger(x_1) \hat{\Psi}_{IX}^\dagger(x_2) V_{dd}(|x_1 - x_2|) \hat{\Psi}_{IX}(x_1) \hat{\Psi}_{IX}(x_2)], \quad (\text{C1})$$

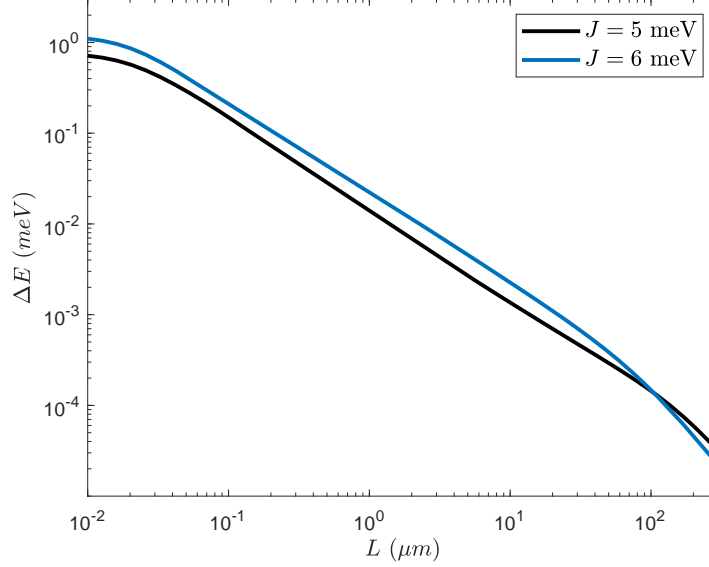


FIG. 7. Numerical calculation for the interaction energy for a system with both direct- and indirect excitons and different values of the inter-exciton coupling strength J .

where IX stands for indirect exciton and X simply for the direct exciton. Here h_{ij}^0 are elements of the matrix h^0 given as

$$h^0(x_k) = \begin{pmatrix} -\frac{\hbar^2}{2m_C} \frac{\partial^2}{\partial x_k^2} + \Delta + \delta_C & \Omega & 0 \\ \Omega & -\frac{\hbar^2}{2m_X} \frac{\partial^2}{\partial x_k^2} & -J \\ 0 & -J & -\frac{\hbar^2}{2m_{IX}} \frac{\partial^2}{\partial x_k^2} \end{pmatrix}, \quad (\text{C2})$$

with equal masses for the two types of excitons. The detunings Δ and δ_C follow the same definitions as in the main text.

In Fig. 7 we show the numerical predictions for the energy shifts as a function of L for $\Omega = 5$ meV and two values of the inter-exciton coupling $J = 5$ and 6 meV. For large L , the system is in the Tonks-Girardeau (TG) regime, and it is seen that for a higher J , the interaction energy gets lowered. At the single-particle level, increasing J gives a larger excitonic component in the lower polariton which in turn increases the effective mass and lowers the TG energy shift at large L . As the confinement length is decreased, the system enters the intermediate regime, which is sensitive to the underlying interaction, and increasing J results in a larger energy shift for a fixed Rabi coupling. In the small L limit, the system decouples from the two-particle basis state consisting of two indirect excitons, and Jaynes-Cummings physics is realized. In this regime, the interaction energy is given as $2f_1(\Omega, J) - f_2(\Omega, J)$, where $f_{1,2}$ are the generalized Rabi couplings with subscript indicating either single- or two-particle system, and it is an increasing function of J .

These additional plots confirm the generality of our conclusions, by showing that the behaviour of the simplest model extends to more complex configurations including several coupled excitonic species.

Appendix D: Coupled wire model

In this final section, we consider a mathematically similar model including a pair of wires. In particular, we assume two kinds of excitons that are distinguished by living on parallel wires and have the possibility of tunneling between them and, in this way, of passing next one another at a not excessive energy cost.

The Hamiltonian is

$$\begin{aligned} \hat{H} = & \sum_{k=1,2} \int dx_k \sum_{i,j=\{C,X_1,X_2\}} \hat{\Psi}_i^\dagger(x_k) h_{ij}^0(x_k) \hat{\Psi}_j(x_k) + \sum_{i=1,2} \frac{1}{2} \int dx_1 dx_2 [\hat{\Psi}_{X_i}^\dagger(x_1) \hat{\Psi}_{X_i}^\dagger(x_2) V_{\text{dd}}(|x_1 - x_2|) \hat{\Psi}_{X_i}(x_1) \hat{\Psi}_{X_i}(x_2)] \\ & + \left\{ \frac{1}{2} \int dx_1 dx_2 [\hat{\Psi}_{X_1}^\dagger(x_1) \hat{\Psi}_{X_2}^\dagger(x_2) V_{\text{dd}}(\sqrt{|x_1 - x_2|^2 + (\Delta z)^2}) \hat{\Psi}_{X_1}(x_1) \hat{\Psi}_{X_2}(x_2)] + h.c. \right\}, \end{aligned} \quad (\text{D1})$$

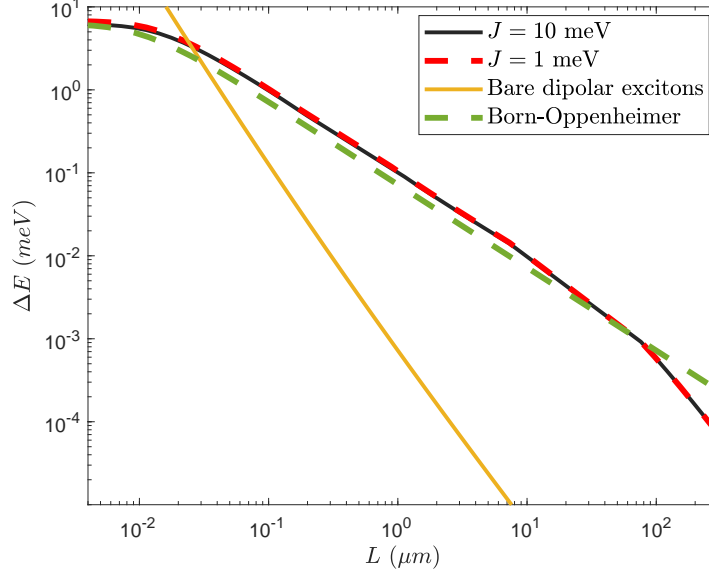


FIG. 8. Numerical calculation for the interaction energy in a quasi-1D system for different values of tunneling strength J . The Rabi coupling is set to $\Omega = 10$ meV. Other parameters as in the figures of the main text.

where h.c. means the hermitian conjugate of the term just before, and h_{ij}^0 are elements of the matrix h^0 given as

$$h^0(x_k) = \begin{pmatrix} -\frac{\hbar^2}{2m_C} \frac{\partial^2}{\partial x_k^2} + \Delta + \delta_C & \Omega & \Omega \\ \Omega & -\frac{\hbar^2}{2m_{X_1}} \frac{\partial^2}{\partial x_k^2} & -J \\ \Omega & -J & -\frac{\hbar^2}{2m_{X_2}} \frac{\partial^2}{\partial x_k^2} \end{pmatrix}, \quad (\text{D2})$$

where the masses of the two excitons are taken to be equal. Note that Δ should be set to the symmetric state of the reduced system

$$\begin{pmatrix} -\frac{\hbar^2}{2m_{X_1}} \frac{\partial^2}{\partial x_k^2} & -J \\ -J & -\frac{\hbar^2}{2m_{X_2}} \frac{\partial^2}{\partial x_k^2} \end{pmatrix} \quad (\text{D3})$$

that is shifted by an additional $-J$ from the bare excitonic energy level, i.e. $\Delta = \epsilon_{X,1} - J - \epsilon_{C,1}$. $\epsilon_{X,1}$ and $\epsilon_{C,1}$ are the lowest excitonic- and photonic single particle states in the confinement potential.

In Fig. 8 we show the numerical results for the interaction energy as a function of the box size L for two values of the tunneling amplitude J and a fixed lateral spacing of $\Delta z = 5$ nm. It is seen that for large L the interaction energy is approximately equal in the two cases. As L is decreased, one sees a slight dependence on J , a smaller J yielding a slightly larger energy shift. This is explained by the fact that at small values of J , the system does not decouple completely from the mixed states $|X_1 X_2\rangle$ and $|X_2 X_1\rangle$ where the two particles are excitons of different kinds. For large values of J , the system completely decouples from these states. This slight dependence on J is more pronounced when Δz is increased. It shows the importance of choosing a large enough J to obtain a realistic quasi-1D model. The energy shift is again J -independent in the quantum dot limit where light is decoupled completely from the states that feature dipolar repulsion.

It is interesting to note that the BO energy shift calculated as discussed in the main text and in the following of the SM is able to accurately capture (green dashed line) the essential physics for intermediate L -values and the quantum dot limit, as for the strict 1D case. Once again, these plots confirm that the qualitative behavior and the order of magnitude of the interaction energy are similar to ones of the purely 1D case discussed in the main text and support our application of the BO formalism to generic geometries beyond 1D.